NEUROSCIENCE

Direct brain recordings reveal prefrontal cortex dynamics of memory development

E. L. Johnson[1,2]*, L. Tang[1,3], Q. Yin[1,3], E. Asano[4], N. Ofen[1,3,5,6]*

Prevailing theories link prefrontal cortex (PFC) maturation to the development of declarative memory. However, the precise spatiotemporal correlates of memory formation in the developing brain are not known. We provide rare intracranial evidence that the spatiotemporal propagation of frontal activity supports memory formation in children. Seventeen subjects (6.2 to 19.4 years) studied visual scenes in preparation for a recognition memory test while undergoing direct cortical monitoring. Earlier PFC activity predicted greater accuracy, and subsecond deviations in activity flow between subregions predicted memory formation. Activity flow between inferior and precentral sites was refined during adolescence, partially explaining gains in memory. In contrast, middle frontal activity predicted memory independent of age. These findings show with subsecond temporal precision that the developing PFC links scene perception and memory formation and underscore the role of the PFC in supporting memory development.

INTRODUCTION

Although children as young as 4 to 6 years do form memories of events in their lives (1, 2), it is widely understood that declarative memory continues to improve into young adulthood (3–6). Declarative memory relies on the dynamic neural communications within a distributed network of brain areas, including regions within the medial temporal lobes and the prefrontal cortex (PFC). Existing evidence indicates that these regions mature at different rates and that the neural correlates of memory may change as children mature into adulthood. Memory development follows a protracted trajectory concomitant with the well-documented maturation of the PFC and widespread neocortical-hippocampal connections (7–10), i.e., the structural substrates of declarative memory in the adult brain. Little is known, however, about the dynamic processes that support memory formation in the developing brain.

There are substantial data on the neural basis of memory in adults, but a paucity of information on how brain development is linked to the emergence of this core ability in children. Drawing evidence from functional magnetic resonance imaging (fMRI) studies comparing children, adolescents, and adults, prevailing theories link the maturation of neural structures such as the PFC to the behavioral gains observed in declarative memory with age (11–15). For example, Ofen and colleagues (11) documented an age-related increase in PFC activation during the study of scenes that were subsequently remembered compared with those that were subsequently forgotten. More recently, Tang and colleagues (12) demonstrated a similar trend in a larger cohort, showing age-related increases in lateral PFC subregions and decreases in superior and medial regions during memory formation. Together, fMRI techniques yield data of superb spatial resolution and evidence age-related increases in lateral PFC activation

coupled with thinning of the cortical gray matter (11, 16), alongside decreases in adjacent superior and medial PFC subregions (12, 17) during memory formation. Given that subregions of the PFC support selective aspects of memory formation (12, 18), it is possible that the functional maturation of specific PFC subregions partially underlies the development of declarative memory.

Until recently, however, it was not possible to detail the precise timing of PFC activity in the developing brain, leaving a critical gap in the understanding of how PFC maturation contributes to declarative memory. Electrocorticographic (ECoG) recordings in patients with surgically implanted subdural electrodes for clinical management of seizures provide a powerful tool for examining the neural basis of human memory (19). Here, we provide rare insight based on data with unprecedented spatiotemporal resolution in the study of neurocognitive development collected from 17 children and adolescents. The ECoG data were cleaned to ensure analyses were performed on electrodes and epochs free of seizure activity (20). Our goal was to examine the subsecond temporal involvement of PFC subregions in memory formation across this sample of children and adolescents. We hypothesized that if the functional specialization of the PFC by subregion underlies declarative memory, then the spatiotemporal propagation of PFC activity by subregion should (i) predict whether a memory forms on a per-trial basis and (ii) vary between individuals according to memory performance. With this work, we provide the first intracranial investigation of memory formation in the developing brain.

We recorded directly from lateral frontal sites in 17 subjects (6.2 to 19.4 years of age; mean ± SD, 13.5 ± 3.5; table S1) while they performed a declarative memory task that has been used previously to study PFC subsequent memory effects in children and adolescents (Fig. 1A) (11, 12, 21). Subsequent memory effects are measured by contrasting the behavioral and/or neural responses recorded during study based on the subsequent fate of the studied material. Contrasting brain activity recorded during the study of scenes that were later remembered to activity recorded during the study of scenes that were later forgotten is a widely used approach to investigate the functional architecture of memory (18). Here, subjects studied sets of 40 pictures of scenes and verbalized a semantic judgment of whether each scene was indoor or outdoor in preparation for a recognition memory

[1]Institute of Gerontology, Wayne State University, Detroit, MI, USA. [2]Helen Wills Neuroscience Institute, University of California, Berkeley, Berkeley, CA, USA. [3]Department of Psychology, Wayne State University, Detroit, MI, USA. [4]Departments of Pediatrics and Neurology, Children's Hospital of Michigan, Wayne State University, Detroit, MI, USA. [5]Merrill Palmer Skillman Institute for Child & Family Development, Wayne State University, Detroit, MI, USA. [6]Neurobiology Department, Weizmann Institute of Science, Rehovot, Israel.
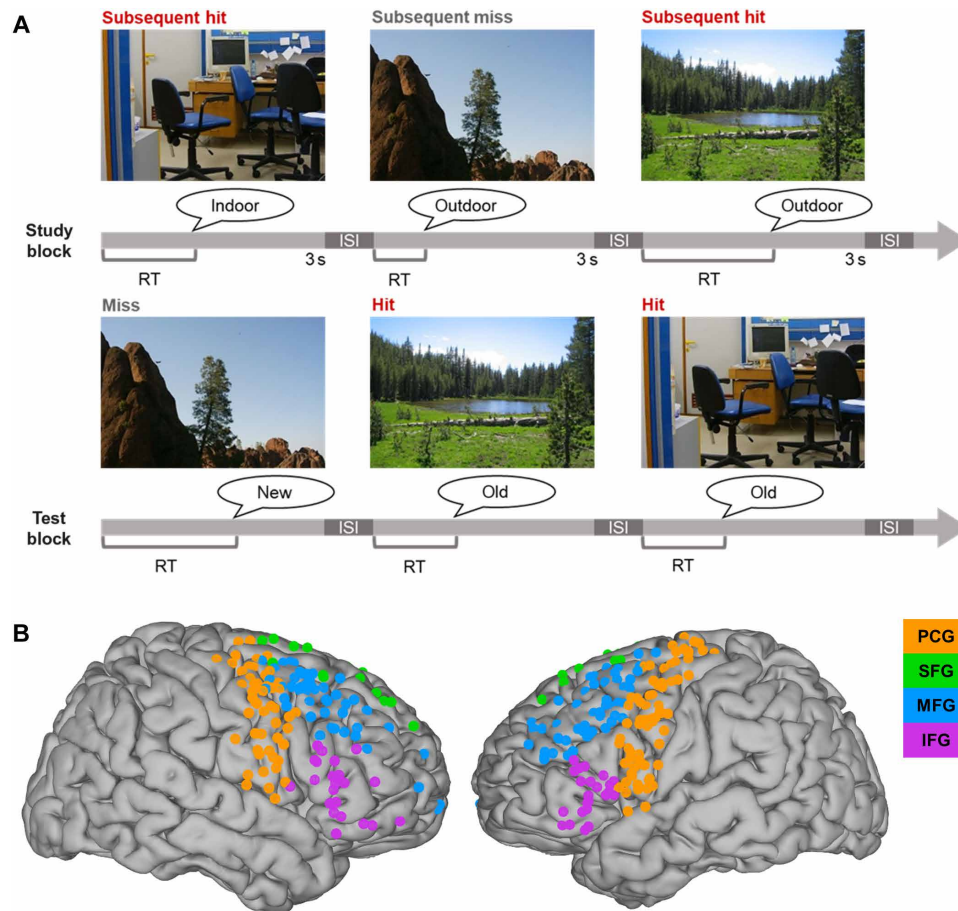*Corresponding author. Email: eljohnson@berkeley.edu (E.L.J.); noa.ofen@wayne.edu (N.O.)

Fig. 1. Subsequent memory paradigm and electrode coverage. (**A**) Subsequent memory paradigm. Subjects studied sets of 40 pictures of scenes (3 s each, separated by a 500-ms interstimulus fixation screen) and made an "indoor"/"outdoor" judgment of each scene in preparation for a recognition memory test of all scenes presented during study, intermixed with 20 new scenes. Subjects made an old/new judgment of each scene during the test block, which was coded as a hit (red), miss (gray; i.e., new response to studied scene), correct rejection, or false alarm (old response to new scene). The test was self-paced. ISI, interstimulus interval (500-ms fixation). Photo credit: Noa Ofen, Individual. (**B**) Reconstruction of active electrode coverage for all subjects (n = 295). Electrodes are color coded by region of interest: orange, PCG; green, SFG; blue, MFG; purple, IFG.

test (all scenes presented at study intermixed with 20 new scenes). Subjects made an "old"/"new" judgment of each scene at test, which was coded as a hit, miss (i.e., new response to studied scene), correct rejection, or false alarm (old response to new scene). This design allowed us to examine the per-trial spatiotemporal propagation of frontal activity by subregion during study as a function of subsequent recognition memory at test (i.e., hit versus miss trials). Furthermore, as a sample size of 17 is large for this type of research, we were also able to examine interindividual variation in the frontal ECoG correlates of memory formation.

We found that subject age did not directly predict the interindividual differences observed in recognition accuracy [accuracy (hit rate − false alarm rate); range, 0.02 to 0.79; $P > 0.15$], making it possible to use age and memory performance as nonredundant variables in the current sample [cf. (*11*, *12*, *21*)]. This divergence between age and memory performance offered a unique opportunity to disentangle individual differences between age, memory, and the frontal ECoG correlates of memory formation. We considered three alternative outcomes of how individual differences in the functional specialization of the PFC might predict individual differences in memory for-

mation during development. In outcome 1, PFC activity would vary as dual functions of age and memory performance, consistent with prevailing theories based on fMRI data, suggesting that PFC activity partially mediates the relationship between age and memory performance. This outcome would thereby provide the first description of PFC subregional involvement in memory development with temporal precision. In outcome 2, activity would vary by memory performance independent of age, revealing temporally precise PFC subregional involvement in memory formation independent of age, thereby challenging prevailing theories implicating protracted PFC maturation in memory development. In outcome 3, activity would vary with age independent of memory, suggesting that age-related differences observed in PFC structure and function may not be directly related to memory performance. If, as we hypothesized, the functional specialization of the PFC by subregion supports declarative memory, then results should favor outcome 1 or 2. We tested these alternatives using a two-tiered, unbiased approach in which frontal ECoG data were first analyzed per trial on the individual subject level and then modeled on the group level using linear mixed-effects models with subjects as random factors, as well as analysis of covariance

(ANCOVA) with individual age and mean recognition accuracy as covariates.

RESULTS
Behavior
We first confirmed that subjects were proficient at the scene encoding task performed during study (rate of correct indoor/outdoor judgments; mean ± SD, 0.91 ± 0.11; chance, 0.5; Fig. 1A and table S1). Study trials with incorrect indoor/outdoor judgments were excluded from further analyses. This important step controls for attention at study. Memory for the attended scenes was assessed in a subsequent recognition test. Of the studied scenes with correct indoor/outdoor judgments, a mean of 0.64 was correctly identified as old (i.e., hit), and the remaining 0.36 was incorrectly identified as new (i.e., miss) (SD, 0.18). Of the scenes used as foils during recognition, a mean of 0.68 was correctly identified as new, and the remaining 0.32 was incorrectly identified as old (i.e., false alarm) (SD, 0.18). Recognition accuracy (hit rate − false alarm rate) varied across subjects from 0.02 to 0.79 (mean ± SD, 0.32 ± 0.22; table S1). ANCOVA was used to model individual differences in accuracy by subject age. Subject age did not covary with accuracy of the encoding task ($P > 0.74$) or the recognition test ($P > 0.15$).

Response times (RTs) on the encoding task performed during study varied across subjects from 763 to 1851 ms (mean ± SD, 1476 ± 331 ms), and RTs at test varied across subjects from 1342 to 4626 ms (mean ± SD, 2602 ± 932 ms; table S1). ANCOVA was again used to model RT data at study and test. We submitted the study RT data to an ANCOVA, with subsequent memory (i.e., hit versus miss) as the grouping variable and individual age and mean recognition accuracy as covariates. There was a main effect of recognition accuracy (uncorrected $P < 0.04$) but no other effects ($P > 0.10$). Post hoc stepwise multiple regression revealed that study RTs were negatively related to recognition accuracy ($b = −811$, $F_{1,32} > 11.05$, $P < 3 \times 10^{-3}$) with no other variables in the model. Test RT data were submitted to an ANCOVA, with stimulus type (i.e., studied versus new) and response accuracy (correct versus incorrect) as grouping variables and age and recognition accuracy as covariates. There were no significant effects ($P > 0.13$).

Task-induced spectral activity
ECoG signals were recorded subdurally from the lateral frontal cortex and denoted according to individual anatomy. Because of the nature of the recording technique, ECoG arrays covered the middle frontal gyrus (MFG) and precentral gyrus (PCG) in 17 of 17 subjects, inferior frontal gyrus (IFG) in 13 of 17 subjects (age range, 10.5 to 19.4 years), and superior frontal gyrus (SFG) in 8 of 17 subjects (11.1 to 19.4 years). We used increases in power at broadband high frequencies (30 to 250 Hz) to track rapid, task-induced cortical activity during scene perception at study. Broadband high-frequency power provides a spatiotemporally precise measure of cortical activity (22–27) and correlates with the fMRI hemodynamic response (28–30), making it ideally suited to bridge the current work with existing fMRI literature. Patterns of high-frequency power at study were assessed per trial as a function of subsequent recognition memory at test.

The multitaper frequency spectrum (31) was calculated for each study trial by sliding a 250-ms window in 25-ms increments across 40 logarithmically spaced frequency bands centered from 30 to 250 Hz ($^1/_3$ fractional bandwidth). We then separated the pretrial base-line (−450 to −150 ms from scene onset) and encoding (−150 to +3000 ms) intervals and performed statistical analysis of task-induced spectral effects by standardizing the encoding outputs on the pretrial baseline via bootstrapping [e.g., (32)]. Task-responsive electrodes were defined per subject by all-trial mean significant increases in power that were sustained for at least 100 ms in at least two contiguous frequency bands during scene presentation at the false discovery rate (FDR) threshold of 0.05 (32, 33). A total of 295 electrodes were selected for analysis (Fig. 1B), with a mean of 17 ± 7 active sites (69 ± 22% of lateral frontal electrodes) per subject. Furthermore, there were no differences in raw power during the pretrial interval between subsequent hit and miss trials (Wilcoxon signed-rank test, FDR-corrected $P > 0.05$), which isolates any subsequent memory effects to spectral activity that was induced by the encoding task at study.

To examine the spatiotemporal patterns of scene perception and memory formation compared with the pretrial baseline, we pooled the per-trial study data from all subjects. For visualization, per-trial task-induced power was averaged across frequencies and intraregional electrode samples within each subject, and trials were sorted by encoding RT (32, 33). As shown in Fig. 2, per-trial cortical activity exhibited subsecond propagation from the PCG, where it preceded the encoding response, to SFG, MFG, and IFG sites, where it appeared more sustained throughout the 3-s scene presentation epoch ($z > 2.57$, $P < 0.01$). Similar spatiotemporal patterns were observed in subsequent recognition hit and miss trials (fig. S1), suggesting that omnibus frontal activity is related to scene perception.

Latency of frontal activity
We assessed the behavioral relevance of the timing of per-trial frontal activity using frequency- and electrode-resolved linear correlation, with the latency of peak activity (i.e., point of maximal neuronal firing and synchrony in local cortical tissue) (22–27) from study scene onset to response onset as the predictor and RT as the outcome. Per-subject linear correlations between the latencies of peak activity and verbal response onset revealed that peak activity was positively timed to the verbal response across all regions in at least 2 of the 40 contiguous frequencies spanning the range of 30 to 250 Hz (99% of active electrode sites per subject, FDR-corrected $P < 0.05$). Frontal activity was observed early on trials in which the study response was verbalized within ~1 s of scene onset and at later latencies for trials with longer RTs, indicating that frontal activity predicted response execution (33). This pattern was especially clear in the PCG, where peak activity preceded the verbal response with an almost fixed duration (Fig. 2A and fig. S1A). The observance of activity even in the 150-ms preceding scene onset on some trials further suggests that the PCG was involved in premotor planning, which was followed quickly by a verbal response [e.g., (32)].

We note that these patterns were evident even in the two youngest subjects (6.2 and 8.5 years of age), who showed broadband peak activity that was significantly timed to the encoding response at all MFG and PCG sites (FDR-corrected $P < 0.05$; Fig. 2, A and B, and fig. S1, A and B). (There was no IFG or SFG coverage in these subjects.) Because individual mean encoding RTs predicted recognition memory accuracy ($P < 3 \times 10^{-3}$), these results evidence that frontal cortex spectral activity at study predicts subsequent recognition at test, even in children.

Group-level ANCOVA was used to model directly the predictive relationship between preresponse frontal peak latencies at study and subsequent recognition accuracy. We submitted the individual peak
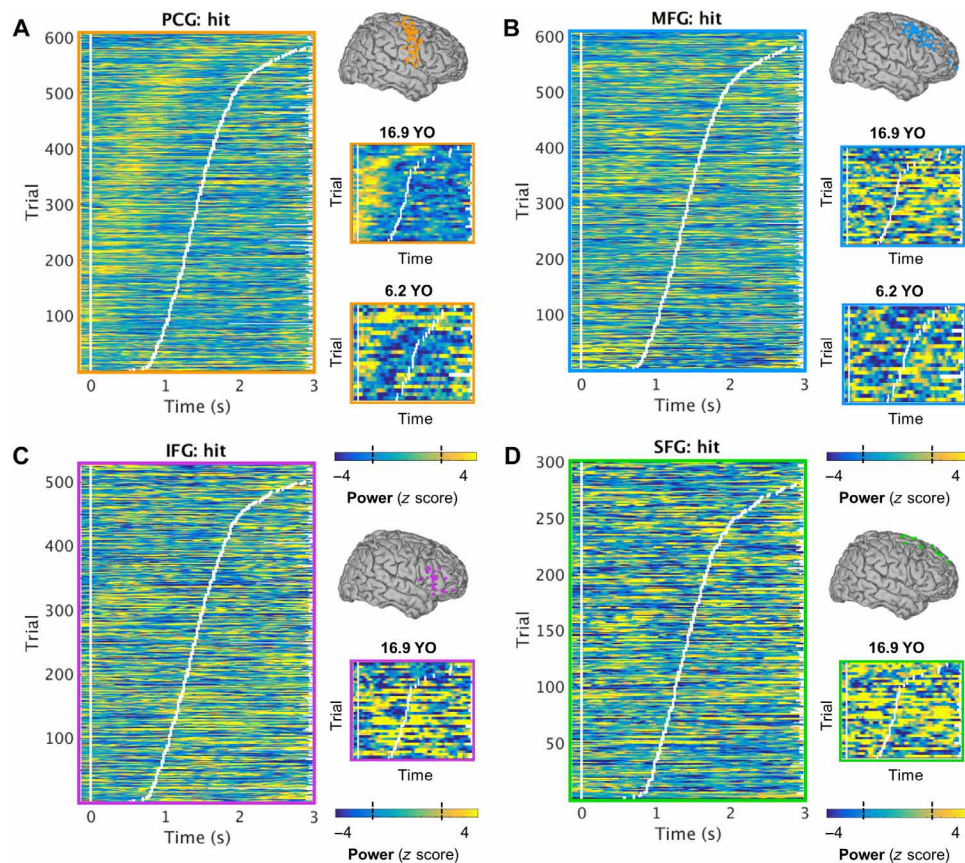
Fig. 2. Frontal activity on subsequent hit trials by region of interest. (**A**) Left: Vertically stacked single hit trials for all subjects sorted by RT (white tick marks), averaged over all active PCG electrodes per subject. Scene onset is indicated by the vertical white line at time = 0 s. Single-trial PCG activity (i.e., z-scored power values compared with a baseline distribution) preceded the response onset ($z > 2.57$, $P < 0.01$). Right: Representative electrode-sample single trials for two subjects aged 16.9 and 6.2 years, showing similar activation patterns regardless of age. The dashed lines on the color bar indicate the threshold of significance ($|z| > 1.96$, $P < 0.05$). YO, years old. (**B**) Equivalent to (A): MFG activity was sustained following the response onset. (**C**) Equivalent to (A): IFG activity was sustained following the response onset. (There was no IFG or SFG coverage in the youngest subject.) (**D**) Equivalent to (A): SFG activity was sustained following the response onset.

latency data to per-region ANCOVAs, with subsequent memory (i.e., hit versus miss) as the grouping variable and age and mean recognition accuracy as covariates. Overall, PCG activity peaked at 699 ± 147 ms (range, 414 to 1001 ms) from scene onset, IFG at 706 ± 162 ms (390 to 1002 ms) from scene onset, MFG at 723 ± 156 ms (392 to 1090 ms) from scene onset, and SFG at 740 ± 176 ms (591 to 1087 ms) from scene onset. There were main effects of accuracy in the MFG, SFG, and PCG models (uncorrected $P < 0.04$; Fig. 3); the relationship did not hold on the group level in the IFG ($P > 0.20$; Fig. 3C). Post hoc stepwise multiple regression revealed that the earlier individual peak activity in the preresponse interval predicted increased subsequent recognition accuracy (PCG: $b = 1266$, $F_{1,30} > 13.34$, $P = 4 \times 10^{-3}$; MFG: $b = -346$, $F_{1,32} > 7.92$, $P < 9 \times 10^{-3}$; SFG: $b = -971$, $F_{1,31} > 15.60$, $P < 5 \times 10^{-4}$). There was also an accuracy × age interaction in the PCG model ($b = -101$, $F_{1,30} > 7.00$, $P < 0.02$; Fig. 3A, right). The negative relationship between PCG peak activity latency and memory accuracy was maximal in adolescent subjects, with no main effect of age ($P > 0.08$). Last, there was a main effect of age in the SFG model ($b = 60$, $F_{1,31} > 14.96$, $P < 6 \times 10^{-4}$; Fig. 3D, left). Like accuracy, age covaried negatively with peak latency, with no interaction or other effects ($P > 0.75$). There were no age effects in the MFG or IFG model (Bonferroni-corrected $P > 0.05$).

Spectral subsequent memory effects

We assessed the relevance of the magnitude of frontal activity to subsequent memory formation, epoched to 3 s from scene onset and time locked to the study response onset, using nonparametric Z tests (10,000 iterations). The empirical subsequent memory effect (i.e., mean z-hit power − mean z-miss power) was compared with a Monte Carlo distribution of chance effects at each time, frequency, and electrode data point, and adjusted for multiple comparisons at the per-subject FDR threshold of 0.05. To visualize the spatiotemporal dynamics of memory-relevant frontal activity, we pooled the time-frequency representations of power from all subjects, averaged across intraregional electrodes separately for hit and miss trials within each subject, juxtaposed with representative electrode-sample statistical subsequent memory effects (Fig. 4). We note that these are the spectral representations of the per-trial data shown in Fig. 2 and fig. S1, demonstrating that overall power is increased across the full frequency range of 30 to 250 Hz during scene encoding.

We then thresholded the time-frequency representations of power at the per-subject FDR and used the intersection of the power and Z test thresholded masks to index subsequent memory effects that reflected task-induced frontal activity. We observed a diverse pattern of spectral subsequent memory effects in all regions, where sites
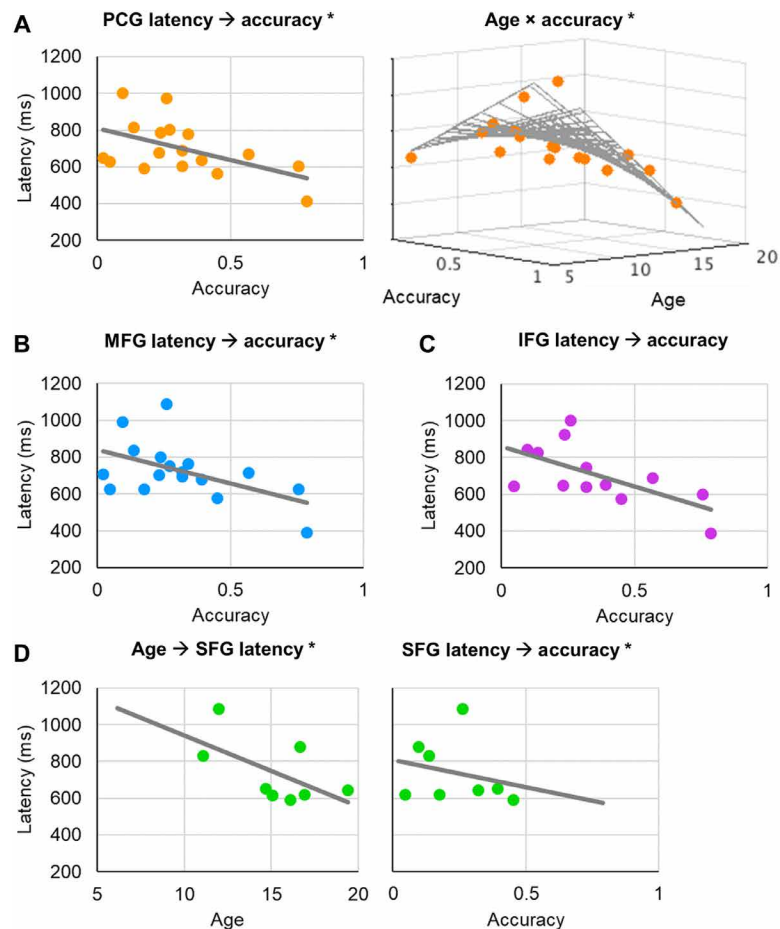
Fig. 3. Frontal peak latency predicts subsequent memory accuracy. (**A**) Left: Preresponse latency of peak PCG activation predicted recognition accuracy ($P = 4 \times 10^{-3}$, $r = -0.52$). Right: The negative relationship between peak PCG activation latency and memory accuracy was maximal in adolescent subjects ($P < 0.02$). Data are represented per subject. *Significant result. (**B**) Equivalent to (A, left): MFG peak activation latency predicted recognition accuracy ($P < 9 \times 10^{-3}$, $r = -0.51$). (**C**) Equivalent to (A, left): Similar, albeit subthreshold, effects were observed in the IFG (full-model ANCOVA $P > 0.20$, $r = -0.63$). (**D**) Left: SFG peak activation latency was predicted by age ($P < 6 \times 10^{-4}$, $r = -0.59$). Right: Equivalent to (A, left): SFG peak activation latency predicted recognition accuracy ($P < 9 \times 10^{-3}$, $r = -0.24$).

exhibiting positive effects were interspersed with sites exhibiting negative effects. At MFG and PCG electrode sites, all 17 subjects exhibited positive effects, and 12 of 17 subjects (71%) also exhibited negative effects, including the two youngest subjects and the oldest subject (6.2, 8.5, and 19.4 years of age; Fig. 4, right insets). At SFG sites, all eight subjects exhibited positive effects, and five of eight subjects (63%) also exhibited negative effects. At IFG sites, 11 of 12 subjects (92%) exhibited positive effects, and 9 of 12 subjects (75%) exhibited negative effects, with 67% overlap.

Last, spectral subsequent memory data were tested on the group level by taking the mean of per-subject significant effects across frequencies and intraregional electrodes in four 1-s epochs between −1500 and +1000 ms relative to the response onset. The outputs were first submitted to per-region linear mixed-effects models, with time as the fixed effect and subjects as random effects. The same data were then submitted to an ANCOVA at each 1-s epoch, with individual age and mean recognition accuracy as covariates. There were no significant group effects ($P > 0.08$), which further evidences the spatiotemporal heterogeneity of frontal activity magnitude effects within individual children and adolescents.

Dynamic inter-regional activity flow

We quantified the temporal interrelationships of task-induced activity between frontal subregions separately for subsequent hit and miss trials, epoched to 3 s from scene onset and time locked to the study response onset, using Spearman's rank partial correlations. Dynamic functional connectivity was characterized by significant power correlations at each time, frequency, and interelectrode data point across serial temporal lags (500-ms data segments, 0- to 475-ms lags in 25-ms steps) (*34*), controlling for the all-electrode mean correlation at each temporal lag. We then analyzed subsequent memory effects using Fisher's Z tests, thresholded the correlation and Z test outputs at the per-subject FDR threshold of 0.05, and used the intersection of the two thresholded masks to index memory-relevant flow of task-induced activity. Outputs were then averaged across frequencies and interregional electrodes to visualize the direction and timing of effects between adjacent subregions, and normalized according to each subject's maximum (Fig. 5 and figs. S2 and S3). We observed reciprocal patterns of activity flow between frontal subregions in all subjects, such that task-induced activity flowed back and forth in both anterior-posterior and superior-inferior directions during memory formation.
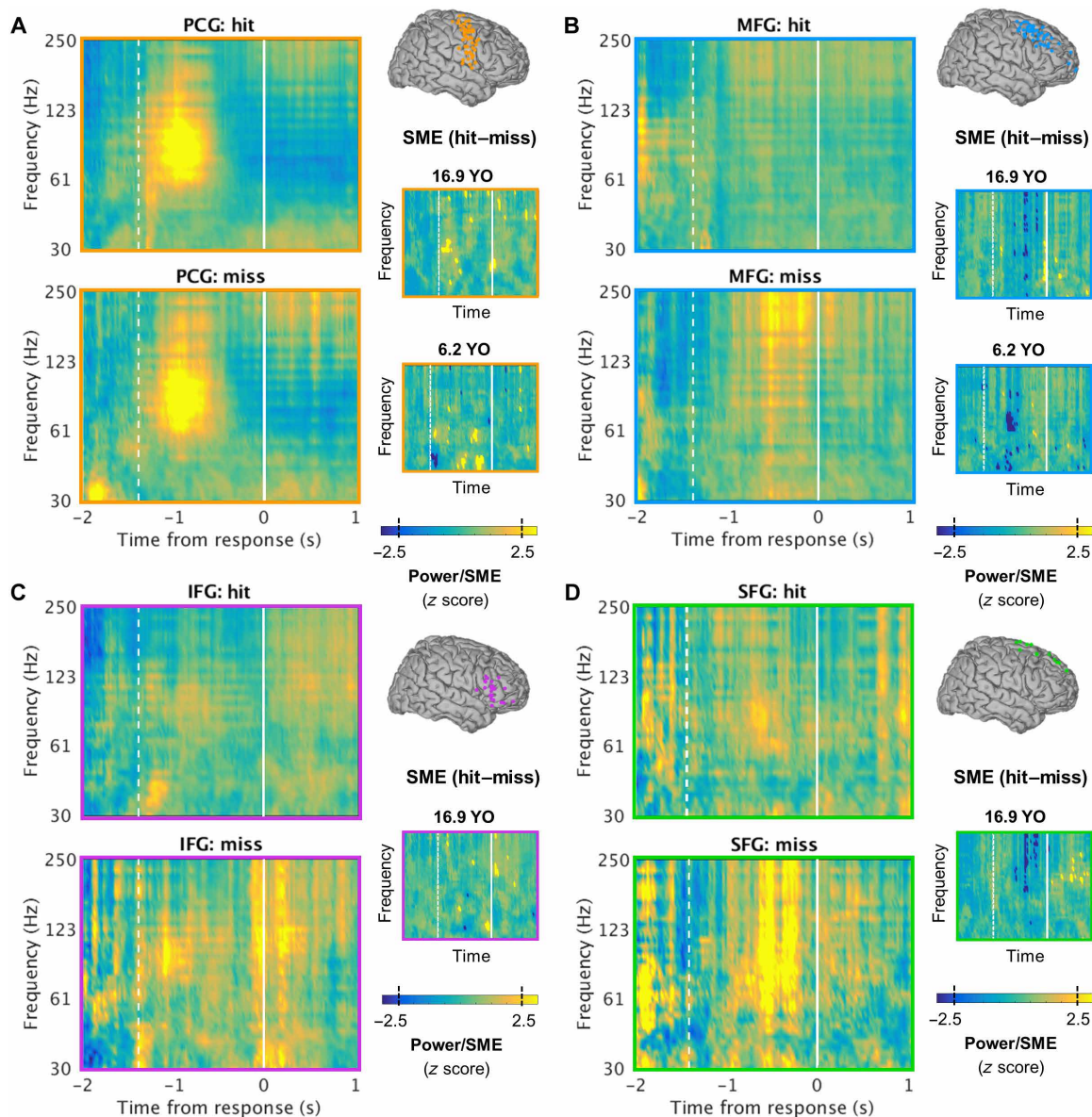
Fig. 4. Spectral subsequent memory effects are spatiotemporally diverse. (**A**) Left: Time-resolved power spectra of subsequent hit (top) and miss (bottom) trials for all subjects, time locked to the RT (time = 0) and averaged over all active PCG electrodes per subject. Response onset is indicated by the vertical white line at time = 0 s, and mean scene onset is indicated by the dashed line. Right: Representative electrode-sample subsequent memory effects (SMEs), masked at the per-subject FDR threshold (i.e., intersection of power and nonparametric Z test masks) for two subjects aged 16.9 and 6.2 years, showing similar effects regardless of age (cf. Fig. 2). Both positive and negative effects were observed. The dashed lines on the color bar indicate the threshold of significance ($|z| > 1.96$, $P < 0.05$). YO, years old. (**B**) Equivalent to (A): Similar effects were observed in the MFG. (**C**) Equivalent to (A): Similar effects were observed in the IFG. (There was no IFG or SFG coverage in the youngest subject.) (**D**) Equivalent to (A): Similar effects were observed in the SFG.

Critically, as we describe below, subsecond deviations in the timing and direction of anterior-posterior activity flow between the PCG and IFG and MFG sites drove subsequent memory formation.

To model the timing and direction of activity flow on the group level, we took the mean of per-subject significant effects across all 25- to 475-ms lags in four 1-s epochs between −1500 and +1000 ms relative to the response onset. The outputs were first submitted to per-region linear mixed-effects models, with time and direction as fixed effects and subjects as random effects. The same data were then submitted to an ANCOVA at each 1-s epoch, with direction as the group-

ing variable and age and mean recognition accuracy as covariates. Overall, memory formation was linked to maximal PCG-to-IFG activity flow at −969 ± 515 ms from response onset (lag, 268 ± 128 ms), followed closely by reciprocal IFG-to-PCG activity flow at −633 ± 727 ms (lag, 202 ± 111 ms; Fig. 5A, top). The linear mixed-effects model revealed main effects of direction ($F_{1,100} > 16.41$, $P < 2 \times 10^{-4}$, $d > 1.65$) and time ($F_{1,100} > 11.89$, $P < 9 \times 10^{-4}$, $d > 1.40$), mediated by a direction × time interaction ($F_{1,100} > 12.21$, $P < 8 \times 10^{-4}$, $d > 1.42$). As shown in Fig. 5A (bottom), these effects reflect a shift in direction over time, uncovering a double dissociation. During successful scene
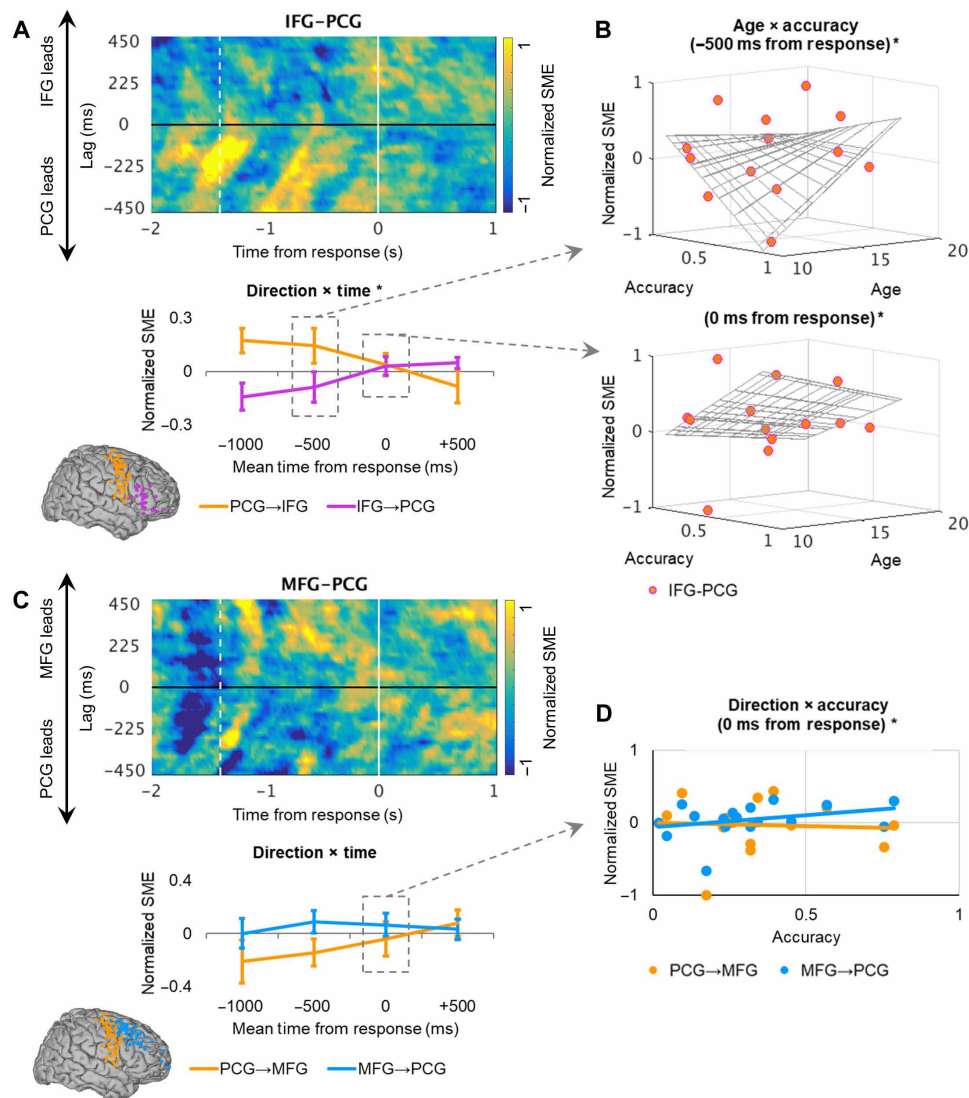
Fig. 5. IFG/MFG-PCG activity flow predicts subsequent memory. (A) Top: Normalized power-correlation subsequent memory effects (SMEs) per temporal lag (25 to 475 ms) for all subjects, time locked to the RT (time = 0 s), masked for at the per-subject FDR threshold (i.e., intersection of partial correlation and Fisher's Z test masks), and averaged over all active IFG-PCG electrode pairs per subject. Response onset is indicated by the vertical white line at time = 0 s, and mean scene onset is indicated by the dashed line. Bottom: Per-second temporal mean power-correlation subsequent memory effects in the PCG-to-IFG (orange) and IFG-to-PCG (purple) directions reveal a shift in direction over time ($P < 9 \times 10^{-4}$). Data are represented as means ± SEM on the group level. *Significant result. **(B)** Time-resolved individual differences in IFG-PCG coactivation. Top: In adolescent subjects, IFG-PCG coactivation increased with mean recognition accuracy preceding the response onset (age × accuracy, $P < 5 \times 10^{-3}$; age, $P < 0.01$; accuracy, $P < 0.02$). Bottom: In middle childhood–aged subjects, IFG-PCG coactivation increased with accuracy at the response onset (age × accuracy, $P < 2 \times 10^{-4}$; age, $P < 7 \times 10^{-4}$; accuracy, $P < 2 \times 10^{-3}$). *Significant result. **(C)** Equivalent to (A): Top: Normalized power-correlation subsequent memory effects per temporal lag for all subjects, averaged over all active MFG-PCG electrode pairs per subject. Bottom: There were no omnibus effects of time or direction between MFG and PCG sites. Orange, PCG-to-MFG; blue, MFG-to-PCG. **(D)** Time-resolved individual differences in MFG-PCG activity flow. Around the response onset (mean, 0 ms), MFG-to-PCG activity flow (blue) predicted mean recognition accuracy (direction × accuracy $P < 0.02$, $r = 0.32$), with no change in PCG-to-MFG activity flow (orange; $r = -0.06$). *Significant result.

memory formation, the PCG led the IFG prior to the response and the IFG led the PCG following the response; when activity flowed in the reverse direction, scenes were subsequently forgotten.

Furthermore, the ANCOVA revealed main effects of individual subject age and mean recognition accuracy on IFG-PCG coactivation (i.e., the point in time at which activity flow shifted in direction). Individual differences in IFG-PCG coactivation were mediated by time-resolved age × accuracy interactions around the response onset (uncorrected $P < 0.03$; Fig. 5B). In adolescent subjects, IFG-PCG

coactivation increased with accuracy immediately preceding the response onset (mean −500 ms: $b = -0.03$, $F_{1,19} > 10.48$, $P < 5 \times 10^{-3}$), and post hoc stepwise multiple regression indicated main effects of age ($b = 5 \times 10^{-3}$, $F_{1,22} > 11.60$, $P < 0.01$) and accuracy ($b = 0.41$, $F_{1,22} > 10.22$, $P < 0.02$) with no other variables in the model. In middle childhood–aged subjects, IFG-PCG coactivation increased with accuracy around the response onset (mean 0 ms: $b = -0.02$, $F_{1,19} > 22.07$, $P < 2 \times 10^{-4}$; age: $b = 4 \times 10^{-3}$, $F_{1,19} > 27.02$, $P < 7 \times 10^{-4}$; accuracy: $b = 0.32$, $F_{1,19} > 22.82$, $P < 2 \times 10^{-3}$). When the shift in direction

occurred in these subjects preceding the response onset, their accuracy decreased, indicating that preresponse IFG-PCG coactivation affected subsequent memory as a function of age. These patterns evidence a system of rapidly shifting and behaviorally relevant activity flow between IFG and PCG sites during memory formation and suggest that adolescents were more flexible in the timing of IFG-PCG coactivation during successful memory formation than children.

Mean peak activity flow overlapped between the MFG and SFG and PCG sites during memory formation, with the MFG leading the PCG at −790 ± 882 ms from response onset (lag, 268 ± 128 ms) and the PCG leading the MFG at −434 ± 824 ms (lag, 282 ± 114 ms), and the SFG leading the PCG at −628 ± 963 ms (lag, 262 ± 165 ms) and the PCG leading the SFG at −659 ± 900 ms (lag, 262 ± 114 ms). No effects were observed in the linear mixed-effects models (MFG-PCG Bonferroni-corrected $P > 0.05$; SFG-PCG $P > 0.71$; Fig. 5C and fig. S2) or the SFG-PCG ANCOVA ($P > 0.06$). However, the MFG-PCG ANCOVA revealed a direction × accuracy interaction around the response onset (mean 0 ms: uncorrected $P < 0.02$; post hoc stepwise multiple regression $b = −0.04$, $F_{1,30} > 7.03$, $P < 0.02$; Fig. 5D). MFG-to-PCG activity flow increased incrementally during memory formation with subsequent recognition accuracy, with no change in PCG-to-MFG activity flow. Individuals with greater accuracy exhibited MFG-to-PCG activity flow at the time of response, regardless of age ($P > 0.91$).

Last, we observed a range of early peak task-induced activity flow in the inferior-to-superior direction, with the IFG leading the MFG at −994 ± 879 ms from response onset (lag, 200 ± 184 ms) and MFG leading the SFG at −631 ± 1010 ms (lag, 153 ± 110 ms). In the reverse direction, SFG-to-MFG activity flow peaked at −731 ± 1010 ms (lag, 191 ± 164 ms), and MFG-to-IFG activity flow peaked at −579 ± 957 ms (lag, 146 ± 121 ms). There were no group-level effects in the IFG-MFG or MFG-SFG models (Bonferroni-corrected $P > 0.05$; fig. S3).

DISCUSSION

The current study demonstrates that the spatiotemporal propagation of PFC activity supports the formation of declarative memories in the developing brain. First, we show behaviorally that the timing of each indoor/outdoor response during the study encoding task (i.e., RT) predicts later memory, as measured by mean recognition accuracy at test. Subjects who executed responses faster exhibited improved memory recognition, and this effect was independent of age. Second, we provide neurophysiological evidence that the per-trial latency of peak task-induced broadband high-frequency power—a proxy for peak neuronal firing and synchrony in local cortical tissue (22–27)—predicts study RT at active frontal sites in all subjects. We then show, on the group level, that the latency of peak MFG, SFG, and PCG activity directly predicts later memory and that adolescents exhibited earlier SFG and PCG peaks than children. Together, these results evidence that the lateral frontal cortex not only provides a critical link between scene perception and response execution (33) but also links this fundamental neurocognitive mechanism to memory formation, even in children.

Third, we observed spatiotemporal heterogeneity in the magnitude of spectral frontal subsequent memory effects across active frontal electrode sites, as measured by statistically significant differences in power on subsequent hit versus subsequent miss trials (18). Within individuals, cortical sites exhibiting positive subsequent memory effects were interspersed with sites exhibiting negative subsequent ef-

memory effects and/or no effects on a fine temporal scale. Across individuals and within each frontal subregion, these patterns did not differ significantly by time relative to response execution (33), subject age, or mean recognition accuracy. These outcomes are consistent with PFC functional heterogeneity or "mixed selectivity" (35), as shown in studies using direct cortical recordings in adults (23, 33, 36) and single-unit recordings in primates (37–39). PFC neuronal populations vary their tuning profiles according to stimulus and response properties, which enables the rapid and flexible perception of different scenes and preparation of semantic judgments. Our data suggest that this cortical flexibility is involved in the success or failure to encode specific scenes into memory (35, 37–41) and is present in children and adolescents.

Fourth, we show that subsecond deviations in the direction of task-induced activity flow between active IFG and PCG sites at study predict whether a scene is subsequently remembered at test (18), as measured by temporal lead/lag relationships in broadband high-frequency power (32, 33). We observed a shift in direction over time, uncovering a double dissociation in dynamic functional connectivity between frontal subregions. During memory formation, the PCG leads the IFG prior to the indoor/outdoor response, and the IFG leads the PCG following the response; when activity flows in the opposite direction, the scene is forgotten. These results indicate that the relative timing of IFG and PCG activity during scene perception predicts subsequent memory.

Furthermore, the timing of the shift in direction—i.e., the point at which the IFG and the PCG are concurrently active at study—predicts recognition memory at test and varies as a function of subject age. In adolescents, top performers exhibited a shift in direction immediately preceding the encoding response, and in middle childhood–aged subjects, top performers exhibited the same shift around the onset of the response. Children who displayed IFG-PCG coactivation before executing an indoor/outdoor response, a mean difference of 500 ms, performed worse at test. Thus, the temporal relationship between the IFG and the PCG is further refined after the age of 10, consistent with the protracted maturational trajectories of frontal regions (7–10). We suggest that this temporal relationship partially supports improved memory with age.

Last, we show that the strength of unidirectional activity flow from active MFG to PCG sites around the onset of the response at study predicts recognition memory at test, independent of subject age. Children and adolescents with high accuracy exhibited increased MFG-led relative to PCG-led activity at the time of response execution during memory formation. Because the timing of activity within the MFG and the relative timing of activity between the MFG and the PCG both predict recognition memory, we provide strong evidence of the importance of the MFG in memory formation. Furthermore, these effects were observed regardless of subject age, evidencing that MFG contributions to declarative memory are sufficient by the age of 6 (1, 6).

The PFC is but one key player in a myriad of developmental changes in the brain and behavior that support gains in declarative memory from childhood through young adulthood (1–6). We propose that these spatiotemporally precise dissociations in the functional specialization of PFC subregions represent the tip of the iceberg in intracranial approaches to the study of memory development. The current study used a scene recognition task that has been used previously to study the PFC correlates of declarative memory in children and adolescents (11, 12, 21), taking care to ensure that the task was appropriate for children and providing reference for task reliability

and interpretation of developmental effects in brain activity. Although the current study also took the requisite steps to ensure artifact-free ECoG data, it is nonetheless important to acknowledge that this sample was clinical by definition. Future intracranial studies should consider not only other neural regions (e.g., hippocampus) [e.g., (16)] but also other tasks that test memory in different ways (e.g., recall) [e.g., (12)].

Conclusions

We report neurophysiological evidence that PFC activity supports memory formation in the developing brain. With unparalleled spatiotemporal resolution, we demonstrate that the timing and magnitude of neuronal activity link scene perception to memory formation within 1 s of scene onset. We further demonstrate that the spatiotemporal propagation of PFC activity guides memory formation such that subsecond deviations in the rapid flow of activity between subregions predict whether a memory is formed. Between IFG and PCG sites, the timing and direction of activity flow determined subsequent memory on a per-trial basis, and this dynamic interrelationship was further refined during adolescence. In contrast, within the MFG, and between MFG and PCG sites, activity predicted overall memory independent of subject age, suggesting that the MFG contributions to memory formation are sufficient by the age of 6. Last, individual subject age did not account for any variation in frontal activity independent of memory. Our findings reveal that the PFC supports memory formation with subsecond temporal precision, even in children, and suggest how selective PFC maturation partially explains developmental gains in memory.

MATERIALS AND METHODS
Experimental design

ECoG arrays are implanted for clinical reasons and, in this sample, were used to monitor children and adolescents with epilepsy in preparation for surgical resection. The purpose of the current study was to examine the spatiotemporal propagation of PFC activity in the developing brain during memory formation. For this reason, we selected 17 subjects from a total pool of 18 based on coverage in the lateral frontal cortex. We made the decision to use broadband high-frequency activity—a proxy for neuronal firing and synchrony in the underlying cortical tissue (22–27)—a priori. Subjects performed a scene subsequent memory task that has been used previously to delineate the functional architecture of memory formation in children (11, 12, 17). ECoG preprocessing routines were performed blinded to anatomical localization and experimental parameters, and the reported results are based on all nonpathologic, artifact-free, lateral frontal electrodes. Data were then analyzed per trial during study as a function of subsequent recognition memory at test (18).

Subjects

We report data from 17 subjects (8 males; 6.2 to 19.4 years of age; mean ± SD, 13.5 ± 3.5) who were undergoing ECoG monitoring as part of clinical management of seizures at the Children's Hospital of Michigan. Written informed consent was obtained from subjects 18 years and older and from the guardians of all subjects younger than 18 years; written assent was obtained from subjects aged 13 to 17 years, and oral assent was obtained from younger children. The Wayne State University Institutional Review Board approved this study in accordance with the Declaration of Helsinki.

Behavioral task

Declarative memory was tested in a study-test task paradigm that has been used previously to study PFC subsequent memory effects in children and adolescents (Fig. 1A) (11, 12, 21). Subjects studied sets of 40 indoor and outdoor scenes, each scene was shown for 3 s, following a 500-ms fixation interval. Subjects were instructed to indicate with a verbal response whether each studied item depicted an indoor or an outdoor scene. Responses were coded as correct or incorrect via offline review of individual audio recordings. A fixation cross remained on screen until a response was provided if none was provided during the 3-s scene presentation epoch. Per-trial RTs were automatically calculated by subtracting the scene onset times from the response onset times. Analysis of electrophysiological data was restricted to correct encoding trials—that is, trials in which scenes were correctly classified as indoor/outdoor, indicating the scenes were properly attended during study. Trials were also considered incorrect if no response was given. A mean of 6 ± 7 trials (range, 0 to 27) per subject were excluded due to incorrect encoding responses.

The memory recognition test included all 40 scenes presented at study, intermixed in a randomized order with 20 new scenes. Each scene remained on screen until a response was given, following a 500-ms fixation pretrial interval. Subjects were instructed to verbalize an old/new judgment of each scene, which was coded as a hit (correct old), miss (new response to old scene), correct rejection (correct new), or false alarm (old response to new scene) via offline review of individual audio recordings. Per-trial RTs were again automatically calculated by subtracting the scene onset times from the response onset times, and trials were excluded if no response was given. Study-test runs were administered in two consecutive cycles of 40 study scenes, followed by 40 studied + 20 new scenes. Half as many new scenes compared with previously studied scenes were introduced in the test phase so that the test remained engaging, and subjects overall responded old and new at roughly equal rates. All subjects completed a short practice run and at least one full study-test run.

On the basis of performance at test, we calculated per subject the hit rate (i.e., number of previously studied scenes that were correctly recognized as old out of all studied scenes) and false alarm rate (number of new scenes presented at test that were incorrectly identified as old out of the number of new scenes presented at test). Recognition accuracy was then calculated as hit rate − false alarm rate, thereby correcting for differences in an individual's tendency to respond old or new (12, 21).

Electrode placement and localization

Platinum macro-electrodes (10-mm intercontact distance, 4-mm diameter) were surgically implanted for extraoperative ECoG recording based solely on the clinical needs of each patient. Three-dimensional electrode reconstructions were created by coregistering postimplantation planar x-ray images of the cortical surface with preoperative T1-weighted spoiled gradient echo magnetic resonance images (42). Automatic parcellation of cortical gyri was performed using Free-Surfer software (43), and electrode sites were assigned anatomical labels (44). Subjects were selected by electrode placement on the lateral frontal cortex, and electrodes were further classified into IFG, MFG, SFG, and PCG regions via group review of individual reconstructions and automatic parcellation results. Electrodes were transformed into standard Talairach space for visual representation across subjects (Fig. 1B).

Data acquisition and preprocessing

ECoG data were acquired using a 192-channel Nihon Kohden Neurofax 1100A Digital System, sampled at 1 kHz. Raw electrophysiology data were filtered with 0.1-Hz high-pass and 300-Hz low-pass finite impulse response filters, and 60-Hz line noise harmonics were removed using discrete Fourier transform. Data traces were demeaned and manually inspected blind to electrode locations and experimental task parameters. Electrodes overlying seizure onset zones (*45*) and electrodes and epochs displaying epileptiform activity or artifactual signal (from poor contact, machine noise, etc.) were excluded. We then epoched the continuous study data blocks into 4-s trials (−1 to +3 s from scene onset), re-referenced every artifact-free electrode to the common average of all artifact-free electrodes, and manually re-inspected the data to reject any trials with residual noise. The final data set included a mean of 26 ± 9 (range, 8 to 41) lateral frontal electrodes and 65 ± 19 (20 to 74) study trials per subject.

Spectral decomposition

Time-frequency representations of power were quantified using a multitapering approach (*31*) with the FieldTrip toolbox (*46*) for MATLAB (MathWorks Inc., Natick, MA). Study data segments were zero padded to 8 s, and the multitaper frequency spectrum was calculated by sliding a 250-ms window in 25-ms increments across 40 logarithmically spaced, partially overlapping frequency bands centered from 30 to 250 Hz, with $^1/_3$ fractional bandwidth at each center frequency. We then separated the baseline (−450 to −150 ms from scene onset) and encoding (−150 to +3000 ms from scene onset) intervals for analysis.

Statistical analysis
Behavior

ANCOVA was used to model encoding task accuracy and recognition accuracy by subject age, and encoding task RTs by subsequent memory (i.e., hit versus miss), age, and recognition accuracy. Recognition test RTs were modeled in a 2 (studied versus new scene) by 2 (correct versus incorrect response) group design, with age and recognition accuracy as covariates. Effects were considered significant if they passed the Bonferroni-corrected threshold for multiple comparisons [i.e., Bonferroni-corrected $\alpha = 0.05/m$ (*m* is the number of main + interaction effects)] (*47*). In cases where effects passed the uncorrected threshold of 0.05, but not the corrected threshold, we used stepwise multiple regression to systematically eliminate variables and reveal independent effects. All ANCOVA and post hoc regression analyses were performed using the MATLAB toolbox MANCOVAN version 1.16 (www.mathworks.com/matlabcentral/fileexchange/27014-mancovan).

Electrode selection

Statistical analysis of task-induced effects was performed per subject by standardizing the encoding power outputs on the pretrial baseline via bootstrapping. Baseline power values were pooled into a single time series for each electrode and frequency, from which we randomly selected and averaged *r* data points (*r* is the number of trials in that subject's data set). This step was repeated 1000 times to create normal distributions of electrode/frequency-resolved pretrial baseline data. Encoding raw power data were *z* scored on the pretrial baseline distributions. This procedure adjusts the power outputs to correct for the 1/*f* power scaling law and reveals activity that is induced, with statistical significance, by the presentation of a scene [for a similar approach, see (*32*, *48*, *49*)]. Task-responsive electrodes were defined by all-trial mean significant increases in power that were sustained for at least 100 ms in at least two contiguous frequency bands during the 3-s scene presentation epoch, adjusted for multiple comparisons over electrodes and frequencies at the per-subject FDR-corrected $\alpha = 0.05$ [e.g., (*32*, *33*)]. A total of 295 lateral frontal electrodes were selected for analysis, with a mean of 17 ± 7 (range, 7 to 32) per subject.

Baseline analysis

The Wilcoxon signed-rank test was used to assess spectral subsequent memory effects (i.e., hit versus miss trials) per subject during the pretrial baseline. Raw power values were averaged over the −450 to −150 ms pretrial interval and tested per electrode and frequency. Effects were adjusted at the per-subject FDR-corrected $\alpha = 0.05$.

Power latency analysis

The predictive relationship between the timing of frontal activity and encoding responses was assessed per subject using linear correlation with FDR correction for multiple comparisons. The per-trial latency of peak task-induced power, prior to the encoding judgment, was indexed per frequency and electrode. The latency of peak activity was defined as the moment of maximal activity occurring at any time point between the onset of the stimulus and the onset of the verbal response. Then, Pearson's correlation was used to test whether the indexed latency of peak power predicted the latency of the encoding response. Effects were adjusted at the per-subject FDR-corrected $\alpha = 0.05$ to correct for multiple comparisons over electrodes and frequencies.

We then used group-level ANCOVA and post hoc stepwise multiple regression to test whether individual mean latency of peak activity, per frontal subregion, predicted recognition accuracy. Peak latency data were submitted to ANCOVAs, with subsequent memory (i.e., hit versus miss) as the grouping variable and subject age and mean recognition accuracy as covariates. In cases where effects passed the uncorrected but not Bonferroni-corrected threshold of 0.05 (*47*), we used stepwise multiple regression to systematically eliminate variables and reveal independent effects.

Spectral subsequent memory analysis

Task-induced power data were tested for subsequent memory effects per subject using nonparametric *Z* tests with FDR correction for multiple comparisons. First, trials with RTs > 3 s were discarded, and all remaining power data segments (0 to +3 s from scene onset) were shifted per trial on the time axis so that the response onset was aligned across trials. The empirical subsequent memory effect was defined as mean *z*-hit power − mean *z*-miss power for each time, frequency, and electrode data point. Then, subsequent hit/miss labels were randomly shuffled using the Monte Carlo method and the subsequent memory effect was recalculated; this procedure was repeated 10,000 times to create a normal distribution of chance effects. Observed subsequent memory effects were considered significant if the empirical effect was significant at the two-tailed $\alpha = 0.05$ (i.e., |*z*-hit − *z*-miss| > 1.96), and fewer than 5% of randomizations yielded a larger effect (corrected $\alpha = 0.05$). Last, we thresholded both the *Z* test outputs and time-frequency representations of power at the per-subject FDR-corrected $\alpha = 0.05$ to correct for multiple comparisons over electrodes, frequencies, and time points. Observed subsequent memory effects were considered significant where positive effects intersected with significant *z*-hit power values, and negative effects intersected with significant *z*-miss power values.

Linear mixed-effects models were used to test the temporal dynamics of subsequent memory effects on the group level (*48*). *Z* test outputs were pooled within each subject across intraregional electrodes

and four 1-s epochs from response onset: −1500 to −500 ms, −1000 to 0 ms, −500 to +500 ms, and 0 to +1000 ms. We computed the mean of all significant subsequent memory effects and submitted the outputs to statistical testing per region, with time epochs as fixed effects and subjects as random effects. We then submitted the same outputs to ANCOVA per frontal subregion and epoch, with subject age and mean recognition accuracy as covariates to assess individual differences.

Inter-regional power lead/lag analysis

Dynamic flow of task-induced power was quantified per subject between all pairs of electrodes in adjacent frontal subregions using nonparametric partial correlations with FDR correction for multiple comparisons. First, trials with RTs > 3 s were discarded and all remaining power data segments (0 to +3 s from scene onset) were shifted per trial on the time axis so that the response onset was aligned across trials, and the trial-wise means were calculated for hit and miss trials. Then, Spearman's rank correlation was computed for each time, frequency, and electrode-pair data point between 500-ms power data segments at each electrode A-B pair by sliding electrode B in 25-ms increments at latencies from 0 to 475 ms following electrode A. For comparable approaches, see (32, 34). We also partialled out the all-electrode mean power at each time-lag increment to minimize the confounding impact of a common reference scheme on connectivity estimates (50). Observed correlation coefficients were considered significant if the P value was significant at the positive-tailed $\alpha = 0.05$, adjusted at the per-subject FDR-corrected $\alpha = 0.05$. Power lag data were then tested for subsequent memory effects using Fisher's Z tests with FDR correction for multiple comparisons (i.e., FDR-corrected $\alpha = 0.05$). Observed subsequent memory effects were considered significant where positive effects intersected with significant P values on hit trials and negative effects intersected with significant P values on miss trials.

Linear mixed-effects models were again used to test the temporal dynamics of subsequent memory effects on the group level (48). Z test outputs were pooled within each subject across inter-regional electrodes and temporal lags from 25 to 475 ms in four 1-s epochs from −1500 to +500 ms relative to the response onset. We computed the mean of all significant subsequent memory effects in each direction (i.e., electrodes A-to-B and B-to-A) and submitted the outputs to statistical testing per region, with direction and time epochs as fixed effects and subjects as random effects. Effects were considered significant at the Bonferroni-corrected threshold of 0.05 (47). We then submitted the same outputs to ANCOVA per region and 1-s epoch, with direction as the grouping variable and subject age and mean recognition accuracy as covariates. When effects passed the uncorrected but not Bonferroni-corrected threshold, we used stepwise multiple regression to systematically eliminate variables and reveal independent effects.

SUPPLEMENTARY MATERIALS

Supplementary material for this article is available at http://advances.sciencemag.org/cgi/content/full/4/12/eaat3702/DC1

Fig. S1. Frontal activity on subsequent miss trials by region of interest.
Fig. S2. SFG-PCG activity flow.
Fig. S3. MFG-IFG/SFG activity flow.
Table S1. Individual patient information and behavior.
References (42–50)

REFERENCES AND NOTES

1. V. Raj, M. A. Bell, Cognitive processes supporting episodic memory formation in childhood: The role of source memory, binding, and executive functioning. *Dev. Rev.* **30**, 384–402 (2010).
2. C. T. Ngo, N. S. Newcombe, I. R. Olson, The ontogeny of relational memory and pattern separation. *Dev. Sci.* **1**, e12556 (2018).
3. N. Ofen, The development of neural correlates for memory formation. *Neurosci. Biobehav. Rev.* **36**, 1708–1717 (2012).
4. N. Ofen, Q. Yu, Z. Chen, Memory and the developing brain: Are insights from cognitive neuroscience applicable to education? *Curr. Opin. Behav. Sci.* **10**, 81–88 (2016).
5. S. Ghetti, S. A. Bunge, Neural changes underlying the development of episodic memory during middle childhood. *Dev. Cogn. Neurosci.* **2**, 381–395 (2012).
6. P. J. Bauer, Toward a neuro-developmental account of the development of declarative memory. *Dev. Psychobiol.* **50**, 19–31 (2008).
7. J. N. Giedd, J. Blumenthal, N. O. Jeffries, F. X. Castellanos, H. Liu, A. Zijdenbos, T. Paus, A. C. Evans, J. L. Rapoport, Brain development during childhood and adolescence: A longitudinal MRI study. *Nat. Neurosci.* **2**, 861–863 (1999).
8. N. Gogtay, J. N. Giedd, L. Lusk, K. M. Hayashi, D. Greenstein, A. C. Vaituzis, T. F. Nugent III, D. H. Herman, L. S. Clasen, A. W. Toga, J. L. Rapoport, P. M. Thompson, Dynamic mapping of human cortical development during childhood through early adulthood. *Proc. Natl. Acad. Sci. U.S.A.* **101**, 8174–8179 (2004).
9. E. R. Sowell, P. M. Thompson, C. M. Leonard, S. E. Welcome, E. Kan, A. W. Toga, Longitudinal mapping of cortical thickness and brain growth in normal children. *J. Neurosci.* **24**, 8223–8231 (2004).
10. C. Lebel, C. Beaulieu, Longitudinal development of human brain wiring continues from childhood into adulthood. *J. Neurosci.* **31**, 10937–10947 (2011).
11. N. Ofen, Y.-C. Kao, P. Sokol-Hessner, H. Kim, S. Whitfield-Gabrieli, J. D. E. Gabrieli, Development of the declarative memory system in the human brain. *Nat. Neurosci.* **10**, 1198–1205 (2007).
12. L. Tang, A. T. Shafer, N. Ofen, Prefrontal cortex contributions to the development of memory formation. *Cereb. Cortex* **28**, 3295–3308 (2018).
13. C. Wendelken, C. L. Baym, A. Gazzaley, S. A. Bunge, Neural indices of improved attentional modulation over middle childhood. *Dev. Cogn. Neurosci.* **1**, 175–186 (2011).
14. A. Maril, R. Avital, N. Reggev, M. Zuckerman, T. Sadeh, L. Ben Sira, N. Livneh, Event congruency and episodic encoding: A developmental fMRI study. *Neuropsychologia* **49**, 3036–3045 (2011).
15. O. E. Güler, K. M. Thomas, Developmental differences in the neural correlates of relational encoding and recall in children: An event-related fMRI study. *Dev. Cogn. Neurosci.* **3**, 106–116 (2013).
16. S. Ghetti, D. M. DeMaster, A. P. Yonelinas, S. A. Bunge, Developmental differences in medial temporal lobe function during memory encoding. *J. Neurosci.* **30**, 9548–9556 (2010).
17. X. J. Chai, N. Ofen, J. D. E. Gabrieli, S. Whitfield-Gabrieli, Development of deactivation of the default-mode network during episodic memory formation. *Neuroimage* **84**, 932–938 (2014).
18. H. Kim, Neural activity that predicts subsequent memory and forgetting: A meta-analysis of 74 fMRI studies. *Neuroimage* **54**, 2446–2461 (2011).
19. E. L. Johnson, R. T. Knight, Intracranial recordings and human memory. *Curr. Opin. Neurobiol.* **31**, 18–25 (2015).
20. L. Rossini, R. Garbelli, V. Gnatkovsky, G. Didato, F. Villani, R. Spreafico, F. Deleo, G. Lo Russo, G. Tringali, F. Gozzo, L. Tassi, M. de Curtis, Seizure activity per se does not induce tissue damage markers in human neocortical focal epilepsy. *Ann. Neurol.* **82**, 331–341 (2017).
21. X. J. Chai, N. Ofen, L. F. Jacobs, J. D. E. Gabrieli, Scene complexity: Influence on perception, memory, and development in the medial temporal lobe. *Front. Hum. Neurosci.* **4**, 21 (2010).
22. D. Hermes, M. Nguyen, J. Winawer, Neuronal synchrony and the relation between the blood-oxygen-level dependent response and the local field potential. *PLOS Biol.* **15**, e2001461 (2017).
23. K. J. Miller, C. J. Honey, D. Hermes, R. P. N. Rao, M. denNijs, J. G. Ojemann, Broadband changes in the cortical surface potential track activation of functionally diverse neuronal populations. *Neuroimage* **85**, 711–720 (2014).
24. E. L. Rich, J. D. Wallis, Spatiotemporal dynamics of information encoding revealed in orbitofrontal high-gamma. *Nat. Commun.* **8**, 1139 (2017).
25. B. O. Watson, M. Ding, G. Buzsáki, Temporal coupling of field potentials and action potentials in the neocortex. *Eur. J. Neurosci.* **48**, 2482–2497 (2018).
26. J. R. Manning, J. Jacobs, I. Fried, M. J. Kahana, Broadband shifts in local field potential power spectra are correlated with single-neuron spiking in humans. *J. Neurosci.* **29**, 13613–13620 (2009).
27. S. Ray, N. E. Crone, E. Niebur, P. J. Franaszczuk, S. S. Hsiao, Neural correlates of high-gamma oscillations (60-200 Hz) in macaque local field potentials and their potential implications in electrocorticography. *J. Neurosci.* **28**, 11526–11536 (2008).
28. R. Mukamel, H. Gelbard, A. Arieli, U. Hasson, I. Fried, R. Malach, Coupling between neuronal firing, field potentials, and fMRI in human auditory cortex. *Science* **309**, 951–954 (2005).
29. C. Jacques, N. Witthoft, K. S. Weiner, B. L. Foster, V. Rangarajan, D. Hermes, K. J. Miller, J. Parvizi, K. Grill-Spector, Corresponding ECoG and fMRI category-selective signals in human ventral temporal cortex. *Neuropsychologia* **83**, 14–28 (2016).

30. F. Khursheed, N. Tandon, K. Tertel, T. A. Pieters, M. A. Disano, T. M. Ellmore, Frequency-specific electrocorticographic correlates of working memory delay period fMRI activity. *Neuroimage* **56**, 1773–1782 (2011).

31. P. P. Mitra, B. Pesaran, Analysis of dynamic brain imaging data. *Biophys. J.* **76**, 691–708 (1999).

32. A. Flinker, A. Korzeniewska, A. Y. Shestyuk, P. J. Franaszczuk, N. F. Dronkers, R. T. Knight, N. E. Crone, Redefining the role of Broca's area in speech. *Proc. Natl. Acad. Sci. U.S.A.* **112**, 2871–2875 (2015).

33. M. Haller, J. Case, N. E. Crone, E. F. Chang, D. King-Stephens, K. D. Laxer, P. B. Weber, J. Parvizi, R. T. Knight, A. Y. Shestyuk, Persistent neuronal activity in human prefrontal cortex links perception and action. *Nat. Hum. Behav.* **2**, 80–91 (2018).

34. A. Adhikari, T. Sigurdsson, M. A. Topiwala, J. A. Gordon, Cross-correlation of instantaneous amplitudes of field potential oscillations: A straightforward method to estimate the directionality and lag between brain areas. *J. Neurosci. Methods* **191**, 191–200 (2010).

35. S. Fusi, E. K. Miller, M. Rigotti, Why neurons mix: High dimensionality for higher cognition. *Curr. Opin. Neurobiol.* **37**, 66–74 (2016).

36. F. Guillem, B. N'Kaoua, A. Rougier, B. Claverie, Differential involvement of the human temporal lobe structures in short- and long-term memory processes assessed by intracranial ERPs. *Psychophysiology* **33**, 720–730 (1996).

37. M. Rigotti, O. Barak, M. R. Warden, X.-J. Wang, N. D. Daw, E. K. Miller, S. Fusi, The importance of mixed selectivity in complex cognitive tasks. *Nature* **497**, 585–590 (2013).

38. M. G. Stokes, M. Kusunoki, N. Sigala, H. Nili, D. Gaffan, J. Duncan, Dynamic coding for cognitive control in prefrontal cortex. *Neuron* **78**, 364–375 (2013).

39. E. Balaguer-Ballester, C. C. Lapish, J. K. Seamans, D. Durstewitz, Attracting dynamics of frontal cortex ensembles during memory-guided decision-making. *PLOS Comput. Biol.* **7**, e1002057 (2011).

40. H. Eichenbaum, Still searching for the engram. *Learn. Behav.* **44**, 209–222 (2016).

41. S. McKenzie, C. Keene, A. Farovik, J. Blandon, R. Place, R. Komorowski, H. Eichenbaum, Representation of memories in the cortical-hippocampal system: Results from the application of population similarity analyses. *Neurobiol. Learn. Mem.* **134**, 178–191 (2016).

42. Y. Nakai, J.-w. Jeong, E. C. Brown, R. Rothermel, K. Kojima, T. Kambara, A. Shah, S. Mittal, S. Sood, E. Asano, Three- and four-dimensional mapping of speech and language in patients with epilepsy. *Brain* **140**, 1351–1370 (2017).

43. R. S. Desikan, F. Ségonne, B. Fischl, B. T. Quinn, B. C. Dickerson, D. Blacker, R. L. Buckner, A. M. Dale, R. P. Maguire, B. T. Hyman, M. S. Albert, R. J. Killiany, An automated labeling system for subdividing the human cerebral cortex on MRI scans into gyral based regions of interest. *Neuroimage* **31**, 968–980 (2006).

44. T. A. Pieters, C. R. Conner, N. Tandon, Recursive grid partitioning on a cortical surface model: An optimized technique for the localization of implanted subdural electrodes. *J. Neurosurg.* **118**, 1086–1097 (2013).

45. E. Asano, C. Juhász, A. Shah, S. Sood, H. T. Chugani, Role of subdural electrocorticography in prediction of long-term seizure outcome in epilepsy surgery. *Brain* **132**, 1038–1047 (2009).

46. R. Oostenveld, P. Fries, E. Maris, J.-M. Schoffelen, FieldTrip: Open source software for advanced analysis of MEG, EEG, and invasive electrophysiological data. *Comput. Intell. Neurosci.* **2011**, 156869 (2011).

47. A. O. J. Cramer, D. van Ravenzwaaij, D. Matzke, H. Steingroever, R. Wetzels, R. P. P. P. Grasman, L. J. Waldorp, E.-J. Wagenmakers, Hidden multiplicity in exploratory multiway ANOVA: Prevalence, consequences, and remedies. *Psychon. Bull. Rev.* **23**, 640–647 (2015).

48. E. L. Johnson, J. N. Adams, A.-K. Solbakk, T. Endestad, P. G. Larsson, J. Ivanovic, T. R. Meling, J. J. Lin, R. T. Knight, Dynamic frontotemporal systems process space and time in working memory. *PLOS Biol.* **16**, e2004274 (2018).

49. E. L. Johnson, C. D. Dewar, A.-K. Solbakk, T. Endestad, T. R. Meling, R. T. Knight, Bidirectional frontoparietal oscillatory systems support working memory. *Curr. Biol.* **27**, 1829–1835.e4 (2017).

50. A. M. Bastos, J.-M. Schoffelen, A tutorial review of functional connectivity analysis methods and their interpretational pitfalls. *Front. Syst. Neurosci.* **9**, 175 (2015).

Science Advances

Direct brain recordings reveal prefrontal cortex dynamics of memory development

E. L. Johnson, L. Tang, Q. Yin, E. Asano and N. Ofen

ARTICLE TOOLS	http://advances.sciencemag.org/content/4/12/eaat3702
SUPPLEMENTARY MATERIALS	http://advances.sciencemag.org/content/suppl/2018/12/17/4.12.eaat3702.DC1
REFERENCES	This article cites 50 articles, 8 of which you can access for free http://advances.sciencemag.org/content/4/12/eaat3702#BIBL
PERMISSIONS	http://www.sciencemag.org/help/reprints-and-permissions

Use of this article is subject to the Terms of Service